Supporting Materials

Raman and Autofluorescence Spectrum Dynamics along the HRG-induced Differentiation Pathway of MCF-7 Cells

Shin-ichi Morita, Sota Takanezawa, Michio Hiroshima, Toshiyuki Mitsui, Yukihiro Ozaki, and Yasushi Sako

Supporting Figures

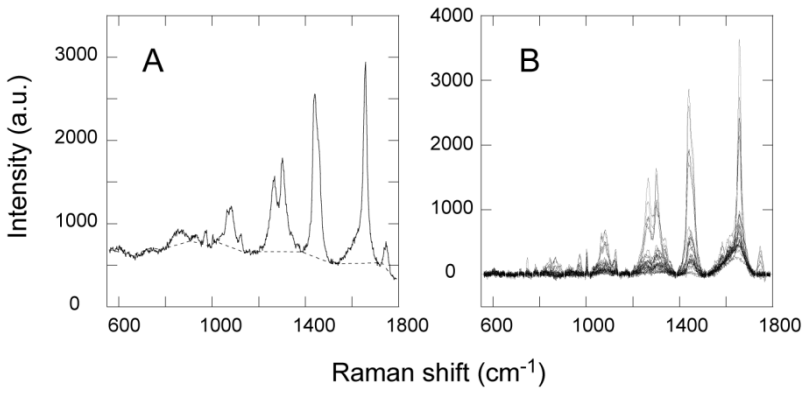

Figure S1. Pretreatments of the photoluminescence spectrum for Raman spectrum analysis

Dark count of the photo-detector was subtracted prior to the acquisition of raw photoluminescence spectra (Fig. 1C in text). In each raw spectrum, 16 points at which Raman signal was small were selected (the wave numbers were 560, 656, 710, 738, 772, 800, 906, 994, 1014, 1140, 1192, 1388, 1518, 1728, 1772, and 1790 cm^{-1}). Raw signals at these points were connected linearly as the background autofluorescence spectrum. (*A*) A typical raw spectrum (*line*) and its autofluorescence background spectrum (dotted line) are shown. After subtraction of the autofluorescence spectrum from the raw spectrum, the remaining spectrum was vector normalized for 616 points (2 cm^{-1}/pint) from 560 to 1790 cm^{-1} (Fig. 2C). The normalized spectra were used for Raman spectrum analysis. *(B)* Randomly selected 25 spectra after autofluorescence subtraction (before vector normalization) are shown among total 243 spectra obtained from cells at various days of differentiation. (The same set of spectra as shown in Fig. 2 is shown.)

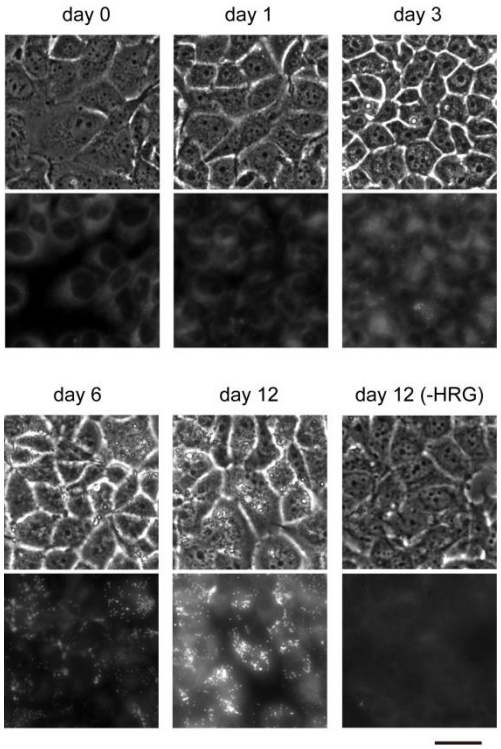

Figure S2. Staining of oil droplets in the cytoplasm of differentiated MCF-7 cells

Cells at indicated days of HRG treatment were stained with BODIPY (Invitrogen) using the Adipocyte Fluorescent Staining kit (Primary Cell, Sapporo, Japan). The upper rows show phase contrast images. The lower rows show fluorescence images acquired at 470–490 nm excitation and 520–550 nm emission wavelengths at the same observation fields in the upper rows. The high refractive index droplets detected in the phase contrast images were oil droplets stained with BODIPY. Cells not stained with BODIPY had no high refractive index droplets. Cells shown in day 12 (–HRG) were not incubated with HRG but with the same amount of PBS (solvent for HRG). No droplet was observed both in phase contrast or fluorescence images in cells without HRG treatment. Bar: 50 μm.

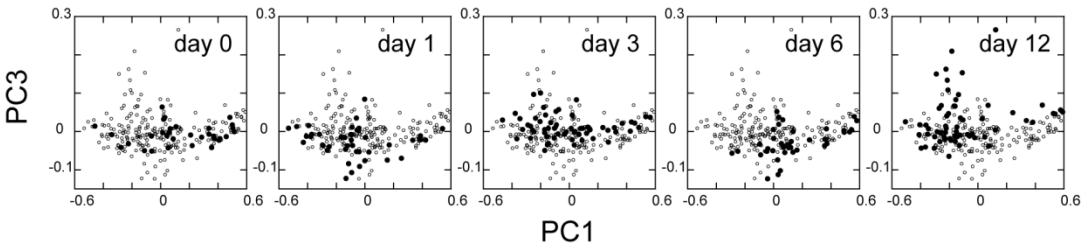

Figure S3. Raman dynamics of cell differentiation in PC1/PC3 plane

Changes of PC3 scores with days of differentiation were plotted in PC1/PC3 plane. Each panel is for the spectra obtained at the indicated day of differentiation (solid dots are for the indicated day, and open dots are for other days for comparison). Oscillation of the PC3 scores is observed with time.

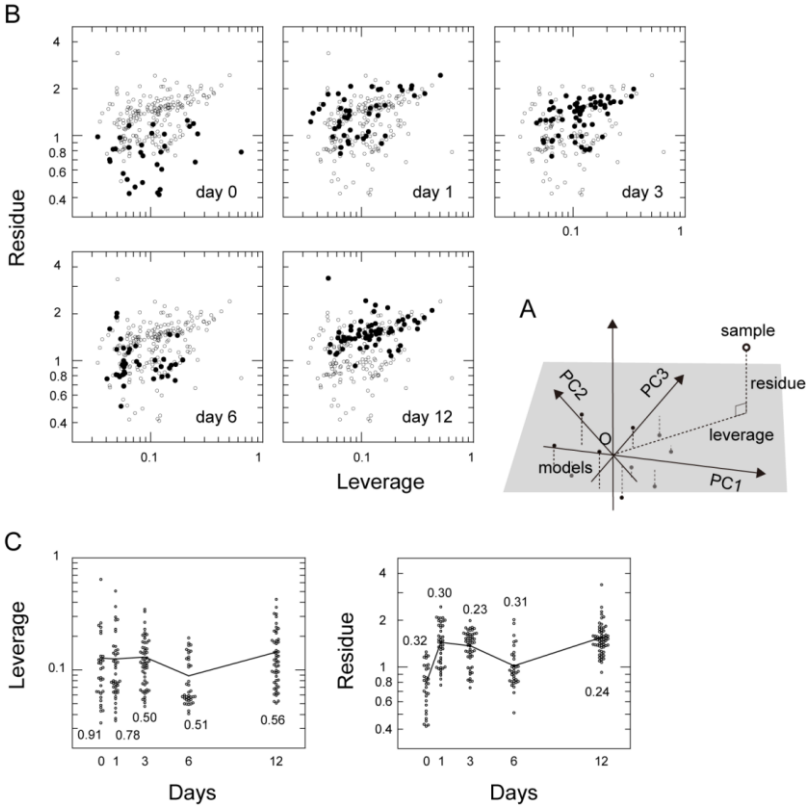

Figure S4. SIMCA analysis and its application to the Raman spectra

(A) To visualize cell differentiation dynamics using entire information in the obtained spectrum, soft independent modeling of class analogy (SIMCA) method was used (Wold 1976). SIMCA method visualizes multi-component data in a two-dimensional plane. We used spectra obtained at day 0 as the model spectra. For the model spectra, principle component analysis (PCA) was carried out, and a hyperplane was determined by PC1–PC4 vectors for the total spectra (Fig. 6), while PC1–PC3 vectors were used for the Raman spectra (Fig. S4B), to calculate the SIMCA plot. Averages of PC scores for the model spectra were set to the coordinates of the origin in the hyperplane. For individual spectra (not only for the model spectra but for all obtained spectra), absolute distance from the origin along the hyperplane was calculated as the leverage value. The distance (absolute value) to the hyperplane from the spectrum was calculated as the residue value. The values of leverage and residue were plotted in a two-dimensional plane (SIMCA plot). Because SIMCA calculates absolute values for both leverage and residue, it detects difference from the average of model spectra but not detects direction of the changes. Difference in the leverage axis roughly means difference of the fractions of major chemical components observed at day 0. Difference in the residue axis roughly means difference in the fractions of minor components and/or appearance of new components. *(B)* SIMCA plot of Raman spectra at the indicated days (solid dots are for the indicated day, and open dots are for other days for comparison). Values of residue changed back and force with time, but changes of leverage were not evident. Distributions of the spectra at day 0 and day 6 were different but not well separated. *(C)* Distributions of the leverage and residue values are plotted with time of HRG treatment. Lines show changes of the average. Numbers are CV (coefficient of variation) values to show the relative variations to the averages.

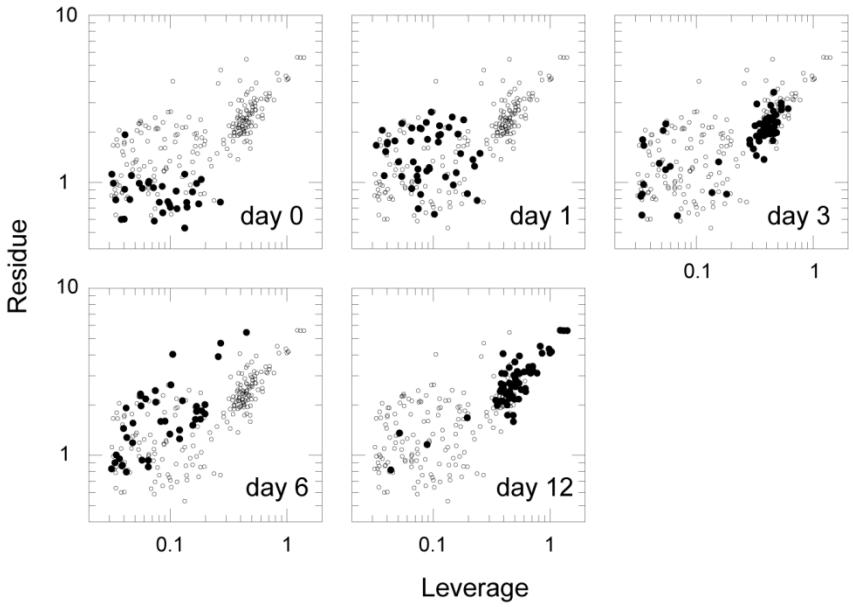

Figure S5. SIMCA analysis of the autofluorescence spectra

SIMCA plot of the autofluorescence spectra at specific days (solid dots represent the indicated day, and open dots represent other days for comparison). The hyperplane for the SIMCA plot was made by PC1 and PC2 of the autofluorescence data. The result was similar to that observed using the entire spectra (Fig. 6 in text) but with worse separation between day 0 and day 1.

Supplement table S1. Assignments of chemical components in Raman spectrum

Raman Shift (cm^{-1})	DNA/RNA[1]	Proteins[1]	Lipids[1]	Carbohydrates[1]	Cytochrome c[2]
602					resonance Raman
620		C-C twist Phe			
642		C-C twist Tyr			
716			$CN^{+}(CH_3)_3$ str		
748					resonance Raman
782	U, C, T ring br				
810	O-P-O str RNA				
828	O-P-O asym str	ring br Tyr			
852		ring br Tyr			
876			C-C-N+ sym str	C-O-H ring	
936		C-C BK str α-helix		C-O-H glycos	
980		C-C BK str β-sheet	C=H bend		
1002		sym ring br Phe			
1030		C-H in-plane Phe			
1082	PO_2^- str		chain C-C str	C-O, C-C str	
1128		C-N str		C-O str	resonance Raman
1156		C-C/C-N str			
1174		C-H bend Tyr			
1208		$C\text{-}C_6H_5$ str Phe, Trp			
1250	T,A	amide III	=CH bend		
1302			CH_2 twist		
1312					resonance Raman
1318	G	CH def			
1338	A, G	CH def		CH def	
1448	G, A CH def	CH def	CH def	CH def	
1574	G, A				
1586					resonance Raman
1604		C=C Phe, Tyr			
1616		C=C Try, Trp			
1658		amide I	C=C str		
1746			C=O ester		

aym, antisymmetrical; BK, backbone; br, breathing, def, deformations; glycos, glycoside bond; in-plane, in-plane deformation; sym, syummetrical; str, stretching

[1] Parker, F. S. (1983), Takai, Y., et al. (1997), Notingher et al. (2004), Huang, Y.-S. et al. (2005)

[2]Hu, S. et al. (1993), Ohshima et al (2010)

References for the Supplement

Hu, S., I. K. Morris, J. P. Singh, K. M. Smith, and T. G. Spiro. 1993. Complete assignment of cytochrome c resonance Raman spectra via enzymatic reconstitution with isotopically labeled heme. *J. Am. Chem. Soc.* 115:12446-12458.

Huang, Y.-S., T. Karashima, M. Yamamoto, and H. Hamaguchi. 2005. Molecular-level investigation of the structure, transformation, and bioactivity of single living fission yeast cells by time- and space-resolved Raman spectroscopy. *Biochemistry.* 44:10009-10019.

Notingher, I., Bisson, I., Bishop, A. E., Randle, W. L., Polak, J. M. P., and Hench, L. L. 2004. In situ spectral monitoring of mRNA translation in embryonic stem cells during differentiation in vitro. *Anal. Chem.* 76:3185-3193.

Ohshima, Y., H. Shinzawa, T. Takenaka, C. Fujita, and H. Sato. 2010. Discrimination analysis of human lung cancer cells associated with histological type and malignancy using Raman spectroscopy. *J. Biomed. Opt.* 15:017009 (1-8).

Parker, F. S. 1983. Applications of infraread, Raman, and resonance Raman spectroscopy in biochemistry. Plenum, New York

Takai, Y., T. Masuko, and H. Takeuchi. 1997. Lipid structure of cytotoxic granules in living human killer T lymphocytes studied by Raman spectroscopy. *Biochem. Biophys. Acta.* 1335:199-208.

Wold, S. 1976. Pattern recognition by means of disjoint principal components models. *Patt. Rec.* 8:127-130.